Particle Imaging Velocimetry (PIV) in partially premixed laminar flames :

Development of a new post-processing algorithm

by

N. Larass[(a)], A. Boukhalfa[(a)], M. Trinité[(a)], D. Honoré[(b)] and P.F. Miquel[1,(b)]

[(a)]*CORIA - UMR 6614 CNRS 76821 Mont-Saint-Aignan Cedex (France)*

[(b)]*Gaz de France, Direction de la Recherche DEG, BP 33, 93211 La Plaine St Denis Cedex (France)*

ABSTRACT

Two-dimensional velocity fields were measured in partially premixed laminar flames using Particle Image Velocimetry (PIV). The velocity measurements were obtained on a multiple slot burner designed with a two-dimensional laminar flow and confined by a combustion chamber with a simplified two-dimensional geometry. These measurements were used to investigate the accuracy of PIV in laminar flames in general, and in partially premixed flames in particular. Focus was placed on measurement accuracy using PIV in the presence of thermophoretic effects and on spatial resolution of PIV image post-processing algorithms.

Images of the flow seeded with refractory particles were obtained for three different flame conditions stabilized on the slot burner using a full-frame CCD camera. The PIV images showed areas of the flow where no particles were detected. The absence of particles in these areas was postulated to be due to the wake of the burner slots and to thermophoresis effects. Thermophoretic velocities were therefore calculated and were found to be on the same order of magnitude than the flow velocity in the vertical direction. Results demonstrate that thermophoresis can induce significant differences between the flow and the particle velocity. Hence caution should be exercised when using PIV in partially premixed laminar flames.

Thermophoresis is also partly responsible for non-homogeneous particle seeding on the PIV images. In areas of the images that were only partially filled with particles, conventional cross-correlation algorithms caused poor spatial resolution due to the assignment of the coordinates of the velocity vector to the center of the correlation window. A specific two-steps post-processing cross-correlation algorithm was therefore developed to increase the accuracy and the spatial resolution of PIV in these areas. This two-steps algorithm was then applied to PIV measurements obtained for the three different partially premixed flame conditions studied here. It was shown that the algorithm did increase the spatial resolution by an order of magnitude.

[1] To whom correspondence should be addressed.

1. INTRODUCTION

Particle Image Velocimetry (PIV) is widely used in reactive flows and combustion environments to measure flow velocities (Wolfrum, 1998 and Gray, 1992). However, up to now, most combustion applications where PIV was used were dealing with turbulent flows (Susset *et al*., 1998 and Honoré *et al*., 2000). Investigators studying turbulent flows were taking advantage of the ability of PIV to measure two-dimensional instantaneous velocity fields. This ability represented a significant improvement over single-point measurement techniques such as Laser Doppler Velocimetry (LDV). In laminar flame investigations, LDV is still frequently used due to its higher spatial resolution. Yet, these investigations could also benefit from PIV in terms of shortening acquisition time and increasing measurement areas. However, when using PIV in laminar reactive flows, one is faced with additional constraints regarding spatial resolution and measurement accuracy.

Partially premixed flames are typically used in household appliances such as domestic boilers (Miquel, 1998). The manufacturers of these type of appliances are faced today with technological challenges to meet the environmental requirements for low pollutant emissions. In order to meet these requirements, it is key to understand the combustion processes in this type of flame. In the course of studying these processes in a simplified version of a commercial household boiler (Miquel, 1998), PIV was used to measure velocities in partially premixed flames. However, we were faced with measurement accuracy limitations due to the presence of thermophoretic effects in the flow and to the limited spatial resolution of the PIV technique.

Hence, a new PIV post-processing cross-correlation algorithm specifically designed for partially premixed laminar flames was developed. It is presented here. It allows increased spatial resolution and measurement accuracy of PIV in laminar flows with inhomogeneous particle seeding. This new PIV algorithm was then applied to three different laminar flame conditions which were used to investigate combustion phenomena in partially premixed flames.

2. EXPERIMENTAL SETUP

2.1. The multiple slot burner

The velocity measurements were obtained using a rectangular seven slot burner designed with a two-dimensional geometry in order to obtain a simplified two-dimensional laminar flow. This multiple slot burner was used previously in the investigation of combustion phenomena in household boilers in the framework of an European Brite-Euram project named TOPDEC (Miquel *et al*., 1998).

A schematic of two of the seven burner slots is shown in Figure 1. Partially premixed flames were stabilized on these burner slots (see Figure 2). They were obtained by introducing a premixed air/methane flow, referred to as primary flow, through the seven slots and a secondary air flow through the eight corresponding inter-slot channels. The flames were protected from entrainment of surrounding air by a combustion chamber closed at the top by a heat exchanger. A chimney was placed on top of the heat exchanger for flue gases exhaust. The walls of the chamber were made of four Vycor™ windows designed for optical free access to the flames and the post combustion zones. This assembly allowed the use of optical non-intrusive measurement techniques. Since the slot burner is two-dimensional, it is characterized by the X and Y axis (see Figure 1). The X axis is the horizontal axis that runs across and perpendicular to the burner slots, whereas the Y axis is the vertical axis. The (X,Y) = (0,0) location corresponds to the geometric center of the central slot, at the slot entrance.

Three flame conditions with identical total output power and total aeration ratio but different primary aeration ratio (air to fuel ratio in the primary flow) were studied. Table 1 presents the operating conditions for the three flames investigated. The total output power was set to 10 kW and the total aeration ratio was 1.4. Operating conditions varied from fully to partially premixed flames, and from fuel-lean to fuel-rich primary flow. For all flame conditions, pure methane was used as fuel.

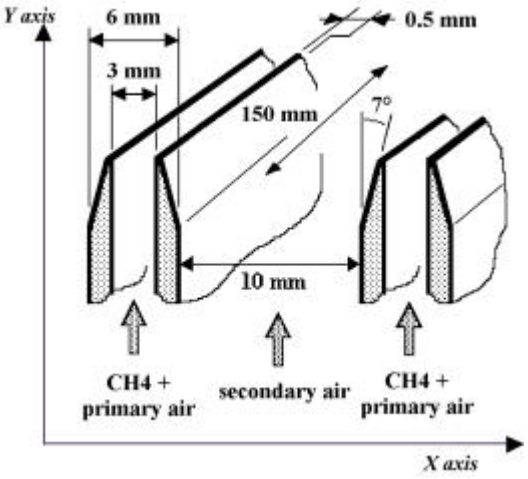

Figure 1: Schematic of two of the seven rectangular burner slots.

Figure 2: Photograph of the multiple slot burner.

Table 1: Operating conditions of the three flames investigated.

Flame Conditions	***Primary Aeration***	***Secondary Aeration***	***Total Aeration Ratio***	***Power Output (kW)***
1	1.4	0.0	1.4	10
2	1.2	0.2	1.4	10
3	0.6	0.8	1.4	10

2.2. The PIV system

Particle Image Velocimetry (PIV) was used to measure the flow velocity in the partially premixed laminar flames studied here. A schematic of the experimental setup of our PIV system is shown in Figure 3. It consisted of a double cavity Nd-YAG laser (Spectra Physics PIV 400), a full frame CCD camera (JAI M-10) with a sensor size of 768 x 574 pixels², a function generator (Stanford Research DS345), an impulse generator (Stanford Research DG535), a color image acquisition card (IC-PCI - module AM-RGB) and a personal computer. Note that the CCD camera used here is a low cost camera designed for industrial needs which yet meets the requirements for high resolution PIV measurements. A laser sheet was formed across the burner slots over a height of 60 mm by using a plano-cylindrical lens (focal length = 40 mm) and a convex lens (focal length = 200 mm). The primary and secondary flows were seeded with particles. In combustion environments, the particles used as tracers for velocity measurements in PIV or LDV systems are typically refractory oxide particles, e.g. Al_2O_3, TiO_2 or ZrO_2 (Melling, 1997). In this study, ZrO_2 particles were chosen for their high refractive index, their high melting point (≈2400 K) and their low mass inertia. Two laser pulses of 8 ns were generated with a total pulse energy of about 400 mJ each. The laser pulses were synchronized with the CCD camera to capture particle image pairs on two full frame images. The field separation signal (VD/2 signal) of the camera was used to synchronize the image acquisition card with the laser pulses using a function generator.

The post-processing of the image pairs was performed by cross-correlation (Lecordier *et al*., 1994). A reference image was first obtained by taking the mean of 50 images recorded without adding the tracer particles in the flow. Then the particles were added and 150 particle images were recorded. It was observed that above 150 image pairs the mean velocity values and the root mean square (RMS) were constant. The reference image was then subtracted from each particle images. This increased the contrast of the particle images and, in turn, resulted in a higher signal to noise ratio (SNR) of the cross-correlation calculation. Cross-correlation calculations were performed with a two dimensional Fast

Fourier Transform (FFT) algorithm with squared interrogation windows (Willert and Gharib, 1991) using the VidPIV© (Optical Flow Systems) software. A total of 150 instantaneous velocity vector fields were obtained. They were further processed by the POP-PIV© software (POst Processing software for Particle Image Velocimetry, licensed by Gaz de France) in order to calculate mean horizontal and vertical velocities and their RMS. The mean horizontal velocity was defined as V_X, whereas the mean vertical velocity was defined as V_Y.

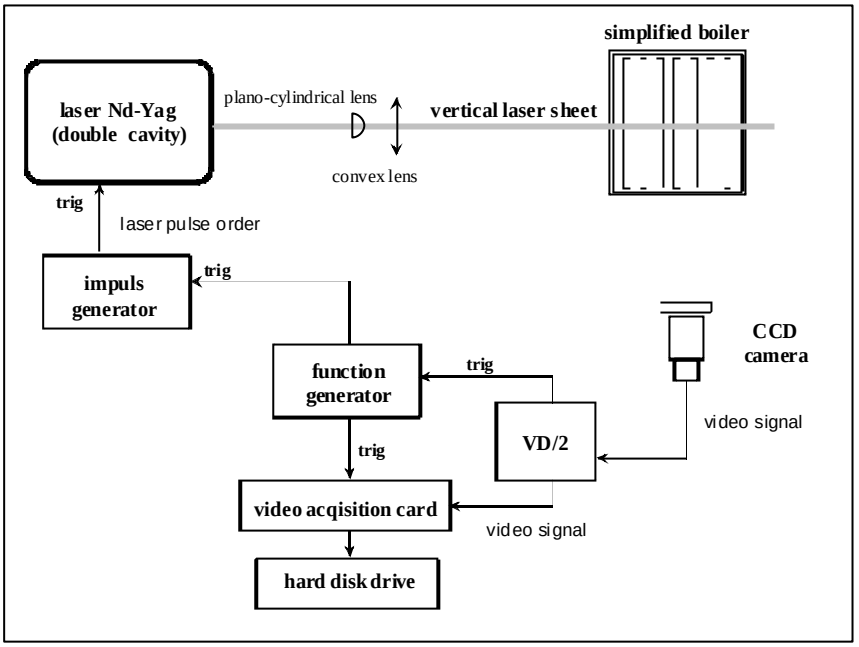

Figure 3: Schematic of the PIV system used in this study.

3. SPECIFIC PIV POST-PROCESSING ALGORITHM FOR LAMINAR FLAMES

3.1. Non-uniform particle seeding

Figure 4a, b and c show a particle image obtained with our PIV system for flame condition #1, 2, and 3, respectively, above one of the seven burner slots, along the X and Y axis. The outline of the burner slot is sketched at the bottom of the images. The bright areas along the bottom line are due to laser light reflections on the slots. As one can see in Figure 4a (i.e., flame condition #1), no particles are detected above the inter-slot channel. This is due to the absence of secondary air flow since flame condition #1 is fully premixed. Regions without particles can also be observed in Figure 4b and c, i.e., flame condition #2 and 3, respectively, between the primary and the secondary stream. One can postulate that the absence of particles between the primary and the secondary stream in these two cases, may be due to the presence of the burner slots: the laminar nature of the flow combined with gas expansion due to the high temperature gradients in this region leaves the wake of the burner slots unseeded.

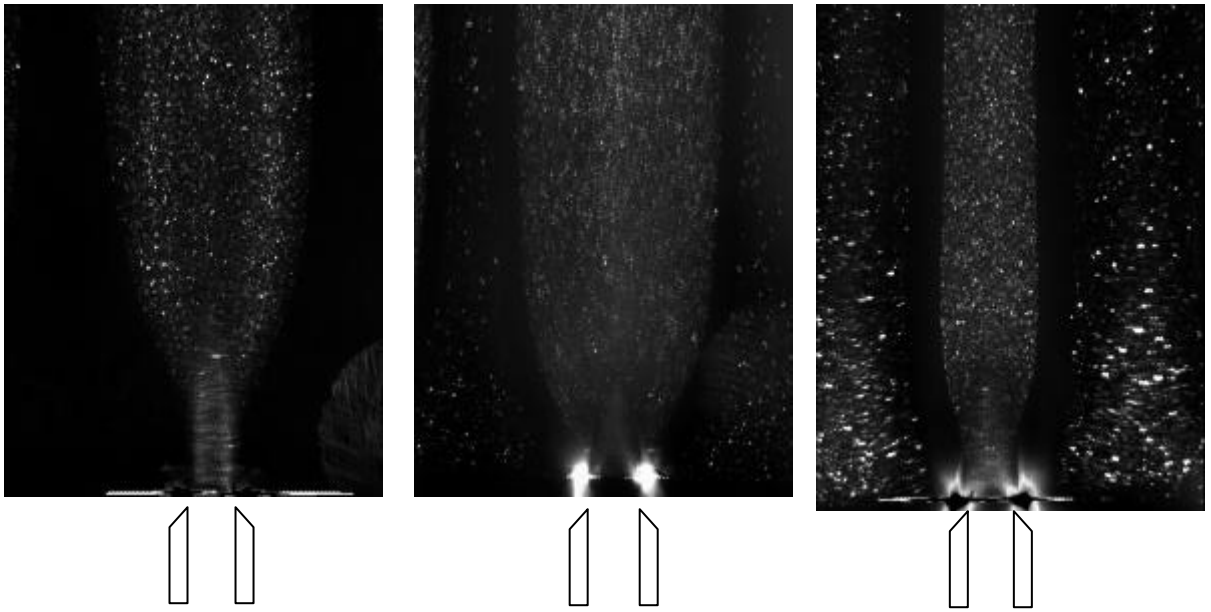

(a) *(b)* *(c)*

Figure 4: Particle images obtained above one burner slot for flame condition #1, 2 and 3, from left to right.

Thermophoretic forces were considered as another possible explanation for the absence of particles between the primary and the secondary stream (Gomez and Rosner, 1993). Thermophoresis is a phenomenon whereby under the influence of a temperature gradient in a gas, an aerosol particle move with constant velocity towards the lower temperature (Waldmann and Schmitt, 1966). The thermophoretic velocity of our ZrO_2 particles was therefore calculated to quantify the effect of thermophoresis on PIV tracer particles in the partially premixed flames studied here. It was also calculated to estimate the influence of thermophoresis on the accuracy of the velocity measurements. In this study the equation proposed by Brock (Brock 1962, and Sung and Law, 1994) was used. Brock's theoretical approach is based on the kinetic theory of gases and gives the thermophoretic velocity as a function of particle size. Note, that the simplified version of Brock's equation presented by Waldmann (Waldmann and Schmitt, 1966) which is often used in combustion investigations can only be used over a short temperature range for ZrO_2 particles due to the high thermal conductivity of this material.

The theoretical thermophoretic velocity V_{th} of the seeding particles is given by Brock (1962) as a function of the thermophoretic force F_{th} :

$$V_{th} = \frac{C}{3p\,\mu d_p} F_{th} \qquad (1)$$

where d_p is the particle diameter, m is the viscosity and C is a correction factor for Stokes' law. C for all Knudsen number is given by the Knudsen -Weber equation:

$$C = 1 + Kn[a + b\,\exp(-g\ /\ Kn)]\ ) \qquad (2)$$

where the Knudsen number, Kn is given as a function of the mean free path l as follows:

$$Kn = \frac{2\,l}{d_p} \qquad (3)$$

The fitting parameters a, b, g are based on experimental data and were taken equal to a = 1.142, b = 0.558, g = 0.999 according to Sung and Law (1994) and Allen and Raabe (1985).

The thermophoretic force F_{th} is given as a function of the gas temperature gradient $\tilde{N}T$ (Brock, 1962, Talbot *et al*., 1980, Sung and Law, 1994):

$$F_{th} = \frac{-6\pi d_p C_s \frac{m^2}{r}\left(\frac{k_F}{k_P} + C_t Kn\right)\frac{\nabla T}{T}}{(1+3C_m Kn)\left(1+2\frac{k_F}{k_P}+2C_t Kn\right)} \qquad (4)$$

where ρ is the gas density, and k_F and k_P are the thermal conductivity of the gas and the particle, respectively. The momentum exchange C_m, the thermal slip C_s and the thermal exchange coefficient C_t were set to $C_m = 1{,}14$, $C_s = 1.17$, $C_t = 2.18$ respectively, according to Talbot *et al.* (1980).

The gas viscosity was calculated using the CHEMKIN© database (Kee *et al.*, 1989), assuming that the gas composition was that of air at all locations. The ZrO_2 particles which were used as seeding particles had a primary particle size of 30 nm and an agglomerate size of about 1 µm. Hence an averaged particle diameter d_p of 1 µm was used in Eq. 4. Note that an increase in particle diameter from 0.2 to 1.0 µm results in an increase of less than 10% of the thermophoretic velocity. The vertical and horizontal temperature gradients were calculated from measurements made by fine wire thermocouples compensated for radiation losses (Miquel *et al.*, 1998, and Larass *et al.*, 1998). They were used to calculate the vertical and horizontal thermophoretic velocity (Larass, 2000).

An example of the effect of thermophoresis in our partially premixed laminar flames is shown in Figure 5 for flame condition #2 (due to space limitations, only the results for flame condition #2 are shown here; the conclusions drawn are identical for the other two flame conditions investigated). Figure 5 shows the two-dimensional graphs of the temperature measured by fine wire thermocouples, the calculated horizontal temperature gradients, the calculated horizontal thermophoretic velocity, and the measured mean horizontal velocity V_X (graph a, b, c, and d, respectively) as a function of the X and Y axis. These graphs were obtained above one burner slot which is drawn schematically along the X axis. On the gray-scale graph of the measured temperature (Figure 5(a)), one can clearly see the presence of a flame front characterized by the sharp temperature gradient above the burner slot (Figure 5(a)). This flame front is the two dimensional premixed flame stabilized on the burner slot. Above the inter-slot channel, the region of increasing temperature is due to the convective heat exchange between the flame and the secondary air flow. Figure 5(b) shows the gray-scale graph of the horizontal temperature gradient defined as $\tilde{N}T$ (see Eq. 4) and calculated from the temperature measurements. As one can see, the two regions of high horizontal temperature gradients are detected on each side of the burner slot centerline (X = 16 mm). They correspond to the two sides of the premixed flame. Note that in these two regions the temperature gradients are of opposite sign.

The two-dimensional gray-scale graph of the theoretical horizontal thermophoretic velocity calculated using Eq. 1 is shown in (Figure 5(c)). As one can see, two regions of high thermophoretic velocity can be observed. They correspond to the regions of high temperature gradients observed in Figure 5(b). Again, note that in these two regions the thermophoretic velocities are of opposite sign. The maximum horizontal thermophoretic velocity, i.e., 0.088 m/s, was calculated at the (X,Y) = (15,2) mm location. If one was to place a particle at this location and if this particle was under the sole influence of thermophoresis, it would be forced towards the centerline of the burner slot. The horizontal component of the velocity, V_X, measured by PIV at the (X,Y) = (15.3,2.02) mm location, i.e., in the vicinity of the (15,2) location, is -0.084 m/s which is on the same order of magnitude than the thermophoretic velocity (see Figure 5(d)). Below the Y= 2 mm plane, V_X could not be measured due to light reflections on the burner slots, but it is expected to be smaller in magnitude than the thermophoretic velocity. Hence, the seeding particles are not allowed to diffuse in the horizontal direction and are prevented from reaching the left hand side of the premixed flame inner cone. By symmetry, the same observations can be made for the left hand side of the premixed flame front. The minimum thermophoretic velocity, i.e., -0.087 m/s, was calculated at the (X,Y) = (17.5,2) mm location. Again, if a particle was placed at this location and if it was under the sole influence of thermophoresis, it would be forced towards the slot centerline. V_X measured by PIV at the (X,Y) = (16.7,202) location, i.e. in the vicinity of the (17.5,2) location is +0.122 m/s which is again on the same order of magnitude and even higher than the thermophoretic velocity. The particles are therefore prevented from reaching the right hand side of the premixed flame inner cone. Moreover, the error caused by thermophoresis on the measured vertical velocity is closed to 100%.

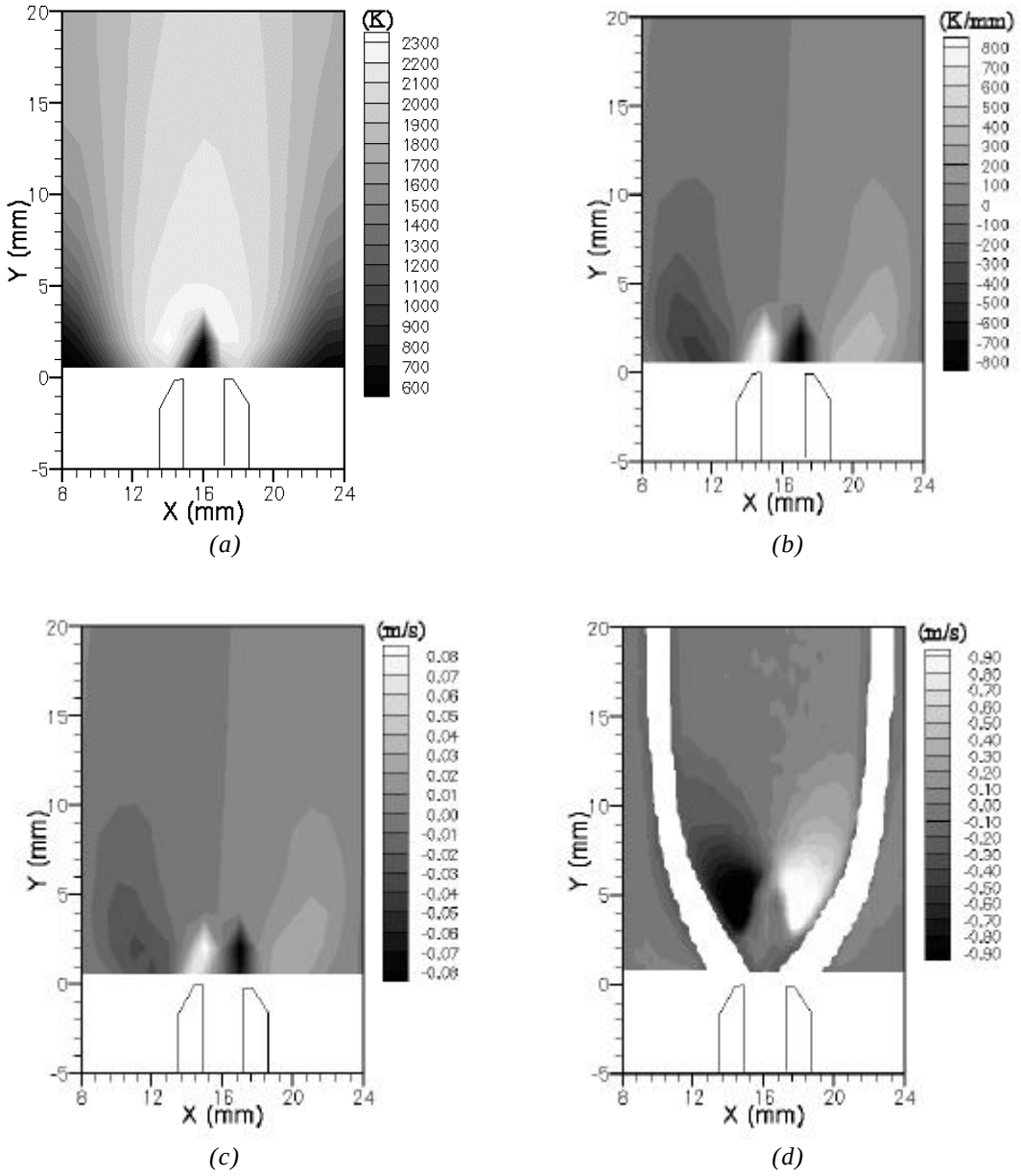

Figure 5: Gray-scale maps of temperature measured by fine wire thermocouples (a), of calculated horizontal temperature gradient (b), of calculated horizontal particle thermophoretic velocity, and of measured horizontal flow velocity V_X (d) for flame condition #2 .

The theoretical vertical component of the thermophoretic velocity was also calculated using Eq. 1. Due to space limitation, the results are not presented here. The vertical component of the thermophoretic velocity is on the same order of magnitude than the horizontal component. Since the maximum measured vertical velocity, $V_{Y,}$ is on the order of a about 1.5 m/s in the areas where the vertical thermophoretic velocity is maximum, the error caused by thermophoresis on the measurements is only around 3%.

3.2. PIV post-processing algorithm for increased spatial resolution

The particle images obtained using PIV in our partially premixed laminar flames showed areas of the flow where no particles were detected. This was postulated to be due to the combined effects of the wake of the burner slots and of thermophoresis. In the areas without particles conventional cross-correlation algorithms cause poor spatial resolution and significant errors in the calculation of the velocity vector. For example, the gray scale images of the flow (see Figure 4) showed that the primary and the secondary streams are clearly separated by an area of the flow where no particles are detected. During the cross-correlation calculation on these images, squared correlation windows which are 32 x 32 pixels² large will be placed over an area of the image which include part of the primary stream, part of the secondary stream and a

dark particle free area. This particle free area can be as wide as 15 pixels. The velocity vector calculated over these windows will therefore have no physical meaning. The solution to this problem is to calculate one velocity vector field for the primary stream and one for the secondary stream. Hence, a specific two-steps post-processing algorithm was developed to increase the accuracy and the spatial resolution of PIV in partially premixed flames.

The first step of our post-processing algorithm consisted of numerically separating the two streams (i.e., the primary and the secondary streams) on the digitized particle images. On a first set of images, the value 0, corresponding to the black color in the gray scale used in our study, was assigned to all pixels outside of the outline of the primary stream. In the same manner, on a second set of images the value 0 was assigned to all pixels outside of the outline of the secondary stream. In both cases the outline of the two streams were defined beforehand using a mean image averaged over 50 particle images. The cross-correlation was then performed on both sets of images to obtain two velocity vector fields, i.e. one field for each stream. The two vector fields were finally reunited in one single data file.

The first step of our post-processing algorithm does not affect the location of the cross-correlation peak. A correlation performed on a window uniformly filled with particles leads to a well-defined correlation peak as shown in Figure 6a. However, if the same calculation is performed on a window which is only partially filled with particles, the shape of the peak is significantly different. Figure 6b shows a correlation peak performed on such a window. In this case the correlation peak appears with a roof like structure. The basis of this roof corresponds to the zero value assigned to the area of the window which is particle free. The rooftop corresponds to the result of a correlation calculation between the value zero of the particle free area and the gray scale values of the particles. In the center of the rooftop, one can distinguish a peak standing out which corresponds to the standard correlation peak. The location of the maximum of this correlation peak with respect to the origin of the correlation window represents the particle displacement. In the flames studied here the horizontal velocities were small therefore the maximum of the peak was always located on the rooftop. Yet, as one can see in Figure 6b, the signal-to-noise ratio between the value of the maximum and the value at the rooftop was small.

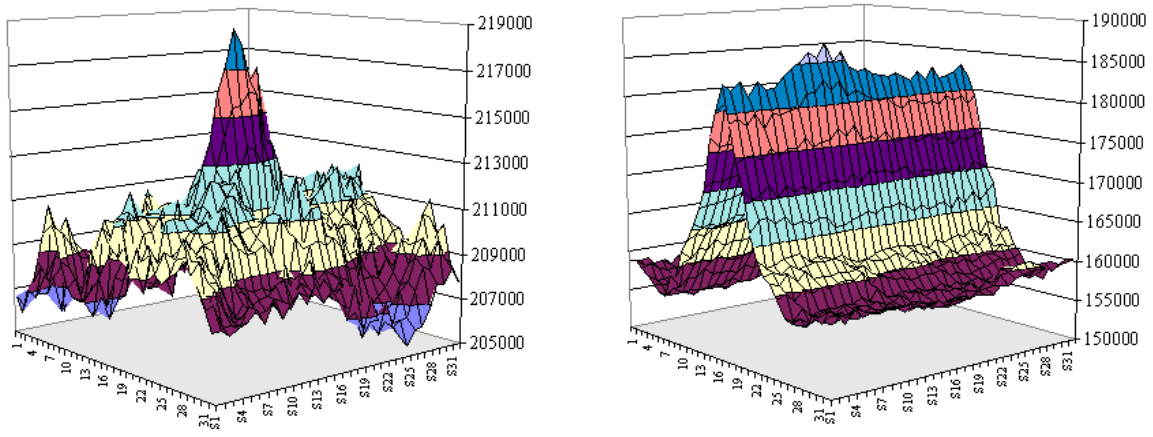

(a) *(b)*

Figure 6: Cross-correlation peak calculated over a 32 x 32 pixel² correlation window:
a) correlation peak calculated over a correlation window with uniform particle repartition;
b) correlation peak calculated over a correlation window with non-uniform particle repartition.

The second step of our post-processing algorithm was developed to increase the spatial resolution of our PIV system in areas with non-uniform particle seeding. The PIV post-processing software used (VIDPIV©, Optical Flow Systems) calculates the most probable particle displacement in a correlation window and from this the most probable velocity vector. It assigns the location of this velocity vector to the center of the correlation window. This assignment is arbitrary but conventional to most PIV software. However, this causes non-trivial spatial resolution biases in the case where the correlation window is located on an area of the flow which is only partially filled with particles. In this case, the center of the correlation window may not correspond to a location where particles were detected. Hence, the geometric center of the window may have no physical meaning. To correct for this, the second step of the post-processing algorithm was developed.

This step of the algorithm first determined the area in each correlation window which was filled with particles. For this, the outline of the primary and secondary streams defined in the first step of the post-processing algorithm were used. For each correlation window, the center of gravity of the area filled with particles was then calculated. Finally, the coordinates of this center of gravity were assigned to the coordinates of the velocity vector.

Figure 7 presents an enlarged area of the two-dimensional graphs of V_Y measured using our PIV system with flame condition #2. These measurements were obtained in an area of the flow only partially filled with particles. As one can see, the velocity field is discontinued. The discontinuity corresponds to a zone where no particles were detected. The high velocity region on the right hand side of the figures corresponds to the location of the premixed flame stabilized above the burner slot, whereas the low velocity region on the left hand side corresponds to location of the secondary air stream. The measurement grid was superposed onto the velocity field in order to show the effect of our post-processing algorithm. Figure 7(a) was obtained by post-processing the PIV measurements with the first step of our two-step algorithm, whereas Figure 7(b) was obtained with the complete two-step algorithm. In Figure 7(a), the area where no particles were detected is outlined by rectangular grid cells giving it a step-like boundary which is inconsistent with the structure of the flow observed in Figure 4(b). In Figure 7(b), the same area is much wider and matches the width of the particle free area observed in the PIV images. Moreover, this area is no longer outlined by rectangular step-like boundaries. The spatial resolution is therefore greatly increased.

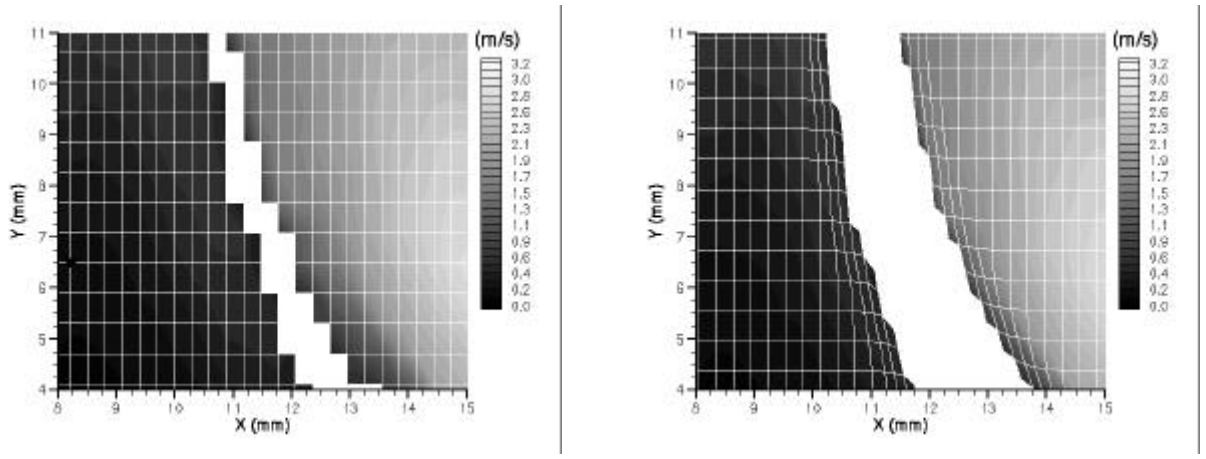

(a) *(b)*

Figure 7: Enlarged area of a gray-scale graph of vertical velocity measurements obtained with flame conditions #2;
a) after applying only the first step of our PIV post-processing algorithm;
b) after applying the first and second step of our PIV post-processing algorithm.

4. RESULTS

Figure 8 shows the two-dimensional gray-scale averaged velocity graphs measured by our PIV system above one burner slot for the three flame conditions studied here as a function of the X and Y axis. The figures on the left side correspond to V_Y, the vertical velocity component, while the figures on the right side correspond to V_X, the horizontal velocity component. These results were obtained after applying the complete two-steps PIV post-processing algorithm presented above. The location of the burner slot is shown schematically on the X axis. As explained previously, the white areas between the primary and secondary streams correspond to areas of the flow where no particles were detected. The contour lines were added on the gray-scale graphs for clarity.

In flame condition #1, i.e., Figure 8(a) and (b), the total flow of gases was injected through the primary slots. This flame condition therefore presents the highest input velocity of all the flame conditions investigated. Above Y = 8 mm, the gas expansion is significant and therefore V_X and V_Y increase. This is due to the high thermal gradients caused by the presence of the flame front. Vertical velocities of up to 3.0 m/s were measured on the centerline of the burner slot at Y = 12 mm. Above this location, V_Y decreases due to the expansion of the flow and to the lower temperature gradients. Horizontal velocities of up to 0.8 m/s were measured along the Y = 10 mm location.

In flame condition #2, i.e., Figure 8(c) and (d), the primary flow is richer than that in flame condition #1, since air is partially injected through the inter-slot channels. The higher laminar flame speed for this fuel/air ratio in the primary flow and the lower input velocity leads to a different flame structure compare to that of flame condition #1. The gas expansion is maximum at Y = 5 mm on both sides of the slot centerline. Note that the highest gas temperatures were not measured on the centerline of the primary slot (see Figure 5(a)) but on both sides of the centerline around X= +15 mm and X = +17 mm. Hence, the highest V_X, i.e., up to 1.2 m/s, were also measured at these locations. Vertical velocities did not exceed 2.5 m/s and were therefore lower than those measured in flame condition #1. In the secondary air stream, V_Y is low at the entrance of the combustion chamber (i.e., around 0.1 m/s on the Y = 2 mm line) but increases along the vertical

direction. This is mainly due to radiation and conductive heat transfer between the burned gases and the secondary air which accelerates the flow, and to the constriction of the secondary flow.

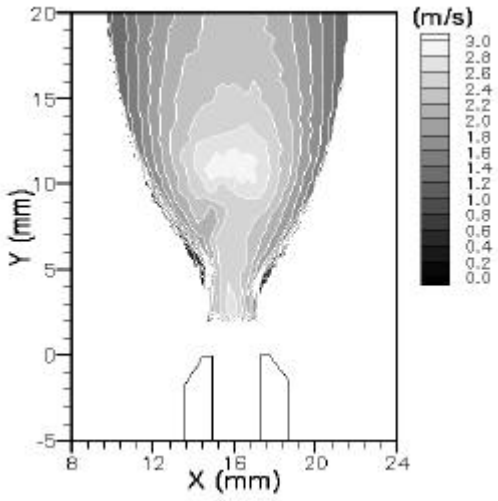

(a)

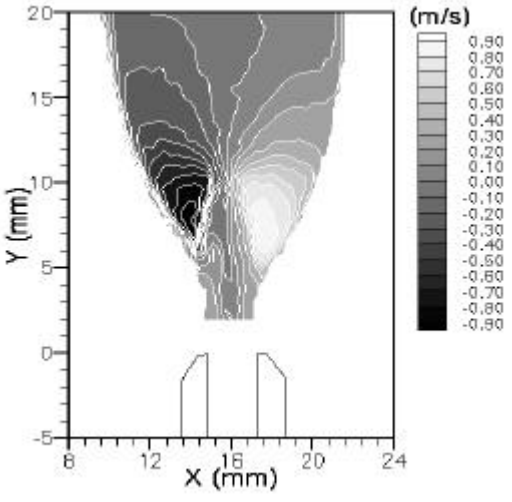

(b)

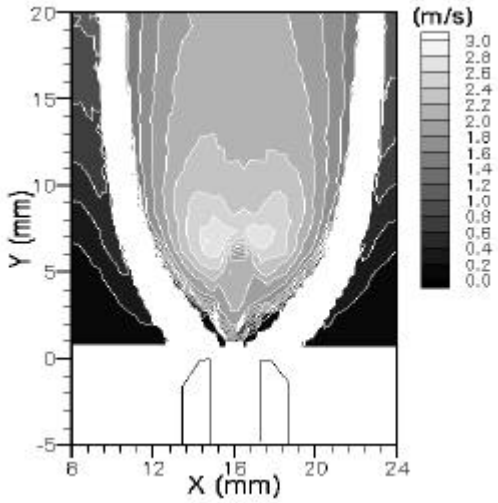

(c)

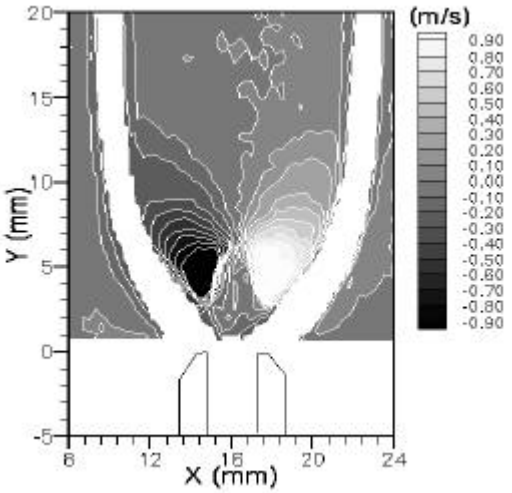

(d)

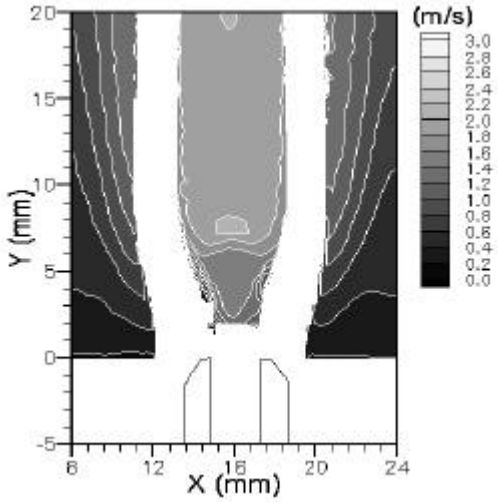

(e)

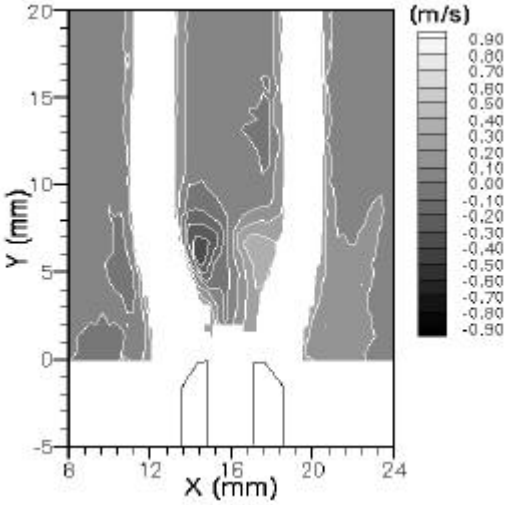

(f)

Figure 8: Two-dimensional gray-scale graph of vertical (left) and horizontal (right) velocity obtained with flame condition #1 (a and b), flame condition #2 (c and d), and flame condition #3 (e and f), respectively.

The measured V_X and V_Y for flame condition #3 are shown in Figure 8(d) and (e). In flame condition #3, most of the air is introduced through the inter-slot channel. Hence, the inlet velocity at the slot entrance is the lowest of the three flame conditions investigated, whereas that at the inter-slot entrance is the highest. Since, most of the air is introduced through the inter-slot channel, the premixed flame stabilized on the burner slot is fuel rich. The combustion is completed by the presence of air diffusing from the secondary stream to the premixed flame. This causes the formation of a diffusion flame on both sides of the premixed flame. This diffusion flame is located in the area of the flow where no particles were detected. The flame structure is therefore quite different from the flame structure observed in the other two flame conditions. Vertical velocities do not exceed 2.0 m/s in the primary stream. Gas expansion in the horizontal direction also remain smaller than for the other two flame conditions. At the Y = 6 mm line, an area where the gases are accelerating can be observed in Figure 8(d) and (e). This is due to the presence of the premixed flame.

5. CONCLUSION

To develop a better understanding of the combustion processes involved in real size household appliances, we initiated a seminal investigation of partially premixed flames which are typically encountered in this type of appliances (Miquel, 1998). As part of this investigation, flow structures were studied for different flame conditions using PIV. The results presented here showed the striking effects of thermophoresis on the accuracy of PIV in our partially premixed flames. For example, the error caused by thermophoresis on the horizontal velocity was on the order of 100%, whereas it was only around 3% on the vertical velocity. The results therefore emphasize that in tracer particle-based velocity measurement techniques, the velocity measured can differ significantly from the gas velocity, particularly in laminar flames. The results also showed that thermophoresis was partly responsible for non-homogeneous particle seeding on the PIV images. To compensate for this, a specific two-step PIV image post-processing algorithm was developed. This algorithm allowed a significant increase in spatial resolution and measurement accuracy compare to conventional PIV post-processing algorithm.

6. ACKNOWLEDGEMENTS

The European Community is gratefully acknowledge for its financial support in the framework of the European TOPDEC project (Brite-Euram CT95-0056).

7. REFERENCES

Allen, M.D. and Raabe, O.G. (1985). "Slip correction measurements of spherical solid aerosol particles in an improved millikan apparatus", Aerosol Sci. and Tech., 4, pp. 269.

Brock, J.R. (1962). "On the theory of thermal forces acting on aerosol particles", Journal of Colloid Science, 17, pp. 768.

Gomez, A. and Rosner, D.E., (1993). "Thermophoretic effects on particles in counterflow laminar diffusion flames", Combust. Sci. and Tech., 89, pp. 335-362.

Gray, C. (1992). "The evolution of particle image velocimetry", IMechE Optical Methods and Data Processing in Heat and Fluid Flow, London, pp.19-35.

Honoré, D. Lecordier, B. Susset, A. Jaffré, D. Perrin, M. Most, J.M. and Trinité, M. (2000). "Time resolved particle image velocimetry in confined bluff-body burner flames", Exp. In Fluids, *in press*.

Kee, R.J. Ruply, K.M. and Miller, J.A. (1989). "Chemkin II - A Fortran chemical kinetics package for the analysis of the gas phase chemical kinetics", Sandia Report SAND89-8009B UC-706.

Larass, N. (2000). "Caractérisation expérimentale des champs thermiques et dynamiques de la combustion dans une chaudière domestique modèle", Thesis, University of Rouen.

Larass, N. Miquel, P.F. Boukhalfa, A. Honoré, D. Perrin, M. and Trinité, M. (1998). "Mesures de vitesses par intercorrelation d'images de particules dans des flammes laminaires d'une chaudière domestique modèle", 6éme Congrès Francophone de Vélocimétrie Laser, St-Louis, France.

Lecordier, B. Mouqallid, M., Vottier, S. Rouland, E. Allano, D. and Trinité, M. (1994). "CCD recording method for cross-correlation PIV developments in unstationary high speed flows", Exp. in Fluids, 17, pp. 205-208.

Melling, A. (1997). "Fundamentals of digital particle image velocimetry", Meas. Sci. and Tech., 8, pp. 1379-1392.

Miquel, P. F. Larass, N. Perrin, M. Lasagni, F. Berghi, M. Hasko, S. Fairweather, M. Hargrave, G. Sherwood, G. Levinsky, H. Mokhov, A. V. de Vries, H. Martin, J. P. Rolon, J. C. Brenez, L. Scouflaire, P. Shin, D.I. Peiter, G. Dreier, T. and Volpp, H.R. (1998). "Detailed measurements in an idealized and a practical natural gas household boiler", International Gas Research Conference, San Diego, USA.

Talbot, L. Cheng, R.K. Schefer, R.W. and Willis, D.R. (1980). "Thermophoresis of particles in a heated boundary layer", J. Fluid Mech., 101, pp. 737-758.

Sung, C.J. and Law, C.K. (1994). "Thermophoretic effects on seeding particles in LDV measurements of flames", Combustion Science and Technology, 99, pp. 119.

Susset, A. Trinité, M. Honoré, D. Jaffré, D. and Perrin, M. (1998). "Experimental investigation of spatio-temporal correlation between aerodynamic and flame front location in an axisymetric non-premixed bluff-body burner flame", 9th International Symposium on Applications of Laser Techniques to Fluid Mechanics, Lisbon, July 13-16.

Waldmann, L. and Schmitt, K. H. (1966). "Thermophoresis and diffusiophoresis of aerosols", Aerosol Science (Davies C.N. ed.), Academic Press, pp. 137-162.

Willert, C. E. and Gharib, M. (1991). "Digital particle image velocimetry", Exp. in Fluids, 10, pp. 181-193.

Wolfrum, J. (1998). "Laser in combustion: from basic theory to practical devices", 27th Symposium (International) on Combustion, The combustion Institute, pp.1-41.